Finite Elements in Analysis and Design 108 (2016) 9–21

Contents lists available at ScienceDirect

Finite Elements in Analysis and Design

journal homepage: www.elsevier.com/locate/finel

The bulk-surface finite element method for reaction–diffusion systems on stationary volumes

Anotida Madzvamuse*, Andy H.W. Chung

University of Sussex, School of Mathematical and Physical Sciences, Department of Mathematics, Brighton BN1 9QH, United Kingdom

ARTICLE INFO

Article history:
Received 8 April 2015
Received in revised form
2 September 2015
Accepted 10 September 2015

Keywords:
Bulk-surface reaction–diffusion equations
Bulk-surface finite elements
Diffusion-driven instability
Pattern formation

ABSTRACT

In this work we present the bulk-surface finite element method (BSFEM) for solving coupled systems of bulk-surface reaction–diffusion equations (BSRDEs) on stationary volumes. Such systems of coupled bulk-surface partial differential equations arise naturally in biological applications and fluid dynamics, for example, in modelling of cellular dynamics in cell motility and transport and diffusion of surfactants in two phase flows. In this proposed framework, we define the surface triangulation as a collection of the faces of the elements of the bulk triangulation whose vertices lie on the surface. This implies that the surface triangulation is the trace of the bulk triangulation. As a result, we construct two finite element spaces for the interior and surface respectively. To discretise in space we use piecewise bilinear elements and the implicit second order fractional-step θ scheme is employed to discretise in time. Furthermore, we use the Newton method to treat the nonlinearities. The BSFEM applied to a coupled system of BSRDEs reveals interesting patterning behaviour. For a set of appropriate model parameter values, the surface reaction–diffusion system is not able to generate patterns everywhere in the bulk except for a small region close to the surface while the bulk reaction–diffusion system is able to induce patterning almost everywhere. Numerical experiments are presented to reveal such patterning processes associated with reaction–diffusion theory.

1. Introduction

Many problems in science and engineering are modelled mathematically by systems of partial differential equations (PDEs). Some of these problems involve coupling surface and interior (bulk) dynamics resulting in coupled systems of bulk-surface PDEs. Such systems arise naturally in many fluid dynamics applications and biological processes. In developmental biology, for example, it is essential the emergence and maintenance of polarised states in the form of heterogeneous distributions of chemical substances (proteins and lipids). Examples of such processes include (but are not limited to) the formation of buds in yeast cells and cell polarisation in biological cells due to responses to external signals through the outer cell membrane [26,27]. In the context of reaction–diffusion processes, such symmetry breaking arises when a uniform steady state, stable in the absence of diffusion, is driven unstable when diffusion is present thereby giving rise to the formation of spatially inhomogeneous solutions in a process now well-known as the Turing diffusion-driven instability [29]. Classical Turing theory requires that one of the chemical species, typically the *inhibitor*, diffuses much faster than the other, the *activator* resulting in what is known as *long-range inhibition, short-range activation* [10,16].

Recently, there has been a surge in studies on models that couple bulk dynamics to surface dynamics. For example, Rätz and Röger [27] study symmetry breaking in a bulk-surface reaction–diffusion model for signalling networks. In this work, a single diffusion partial differential equation (the heat equation) is formulated inside the bulk of a cell, while on the cell-surface, a system of two membrane reaction–diffusion equations is formulated. The bulk and cell-surface membrane are coupled through a Robin-type boundary condition and a flux term for the membrane system [27]. Elliott and Ranner [8] study a finite element approach to a sample elliptic problem: a single elliptic partial differential equation is posed in the bulk and another is posed on the surface. These are then coupled through Robin-type boundary conditions. Burman et al. [4] recently developed cut finite element methods for coupled bulk-surface problems. In this article, single time-independent elliptic parabolic equations are coupled in the bulk and surface through non-zero flux boundary conditions. A trace finite element method has recently been proposed to study a class of coupled bulk-interface transport problems posed on evolving volumes and surfaces [12]. Again, coupling of the bulk and surface dynamics is through non-zero boundary conditions. Novak et al. [24] present an algorithm for solving a diffusion equation on a curved surface coupled

* Corresponding author.
E-mail addresses: a.madzvamuse@sussex.ac.uk (A. Madzvamuse), a.chung@sussex.ac.uk (A.H.W. Chung).

http://dx.doi.org/10.1016/j.finel.2015.09.002

to a diffusion model in the volume. Checkkin et al. [6] study bulk-mediated diffusion on planar surfaces. Again, diffusion models are posed in the bulk and on the surface coupling them through boundary conditions. In the area of tissue engineering and regenerative medicine, electrospun membrane are useful in applications such as filtration systems and sensors for chemical detection. Understanding of the fibres' surface, bulk and architectural properties is crucial to the successful development of integrative technology. Nisbet et al. [23] present detailed review on surface and bulk characterisation of electrospun membranes of porous and fibrous polymer materials. To explain the long-range proton translocation along biological membranes, Medvedev and Stuchebrukhov [22] propose a model that takes into account the coupled bulk-diffusion that accompanies the migration of protons on the surface.

In most of the work above, either elliptic or diffusion models in the bulk have been coupled to surface-elliptic or surface-diffusion or surface-reaction–diffusion models posed on the surface through Robin-type boundary conditions [6,8,22–24,26,27]. Here, our focus is to couple systems of reaction–diffusion equations posed both in the bulk and on the surface, setting a mathematical and computational framework to study more complex interactions such as those observed in cell biology, tissue engineering and regenerative medicine, developmental biology and biopharmaceutical [6,8,22–24,26,27].

The coupled system of bulk-surface reaction–diffusion equations (BSRDEs) may be numerically solved using various discretisation schemes and techniques. We choose to employ the bulk finite element method [9] to numerically solve the bulk-reaction–diffusion system while the surface finite element method [7] is employed to compute numerical solutions corresponding to the surface-reaction–diffusion system. The key idea of the finite element method is that two finite element spaces are constructed, the bulk and surface finite element spaces, by taking a set of all continuous piecewise polynomial functions on each bulk simplex or boundary face element [8]. The bulk and surface reaction–diffusion systems are coupled through Robin-type boundary conditions. The coupled bulk-surface finite element algorithm is implemented in **deal.II** [1].

Other plausible numerical methods for solving such systems include (but are not limited to) finite volume methods [5], particle methods using level set descriptions of the surface [11,14] and closest-point methods [18,19].

Our article is therefore structured as follows. In Section 2 we present the coupled bulk-surface reaction–diffusion system on stationary volumes with appropriate boundary conditions coupling the bulk and surface partial differential equations. Within this section, we give some specific examples of the applications of the coupled system of PDEs. The bulk-surface finite element framework is presented in Section 3. Here we describe how the two finite element spaces are constructed to enable us to carry out the spatial discretisation of the model system. We also detail how the bulk and surface triangulations are carried out. To discretise in time, we use the fractional-step θ method coupled with the Newton method to treat nonlinearities arising from the nonlinear reactions. Numerical experiments are presented in Section 4 where we discuss how bulk dynamics influence patterning on the surface and vice versa. We conclude and discuss the implications of our studies in Section 5 as well as setting foundations for future research.

2. Coupled system of bulk-surface reaction–diffusion equations (BSRDEs) on stationary volumes

In this section we present our model system which comprises a system of coupled bulk-surface reaction–diffusion equations (BSRDEs) posed in a three-dimensional volume as well as on its surface. We impose boundary conditions on the system of reaction–diffusion equations in the interior of the volume that couple internal dynamics to surface dynamics. Since we are interested in closed surfaces (whose boundary is empty) then the system of reaction–diffusion system on the surface is devoid of boundary conditions.

2.1. Notation

Let Γ be a closed, compact and smooth hypersurface without boundary in $\mathbb{R}^{N+1}$ enclosing a convex volume Ω. Let $\boldsymbol{n}$ denote the unit outer normal to Γ, and let U be any open subset of $\mathbb{R}^{N+1}$ containing Γ, then for any function u which is differentiable in U, we define the tangential gradient on Γ by

$$\nabla_\Gamma u = \nabla u - (\nabla u \cdot \boldsymbol{n})\boldsymbol{n},$$

where $\cdot$ denotes the dot product and ∇ denotes the gradient in $\mathbb{R}^{N+1}$. The tangential gradient is the projection of the gradient onto

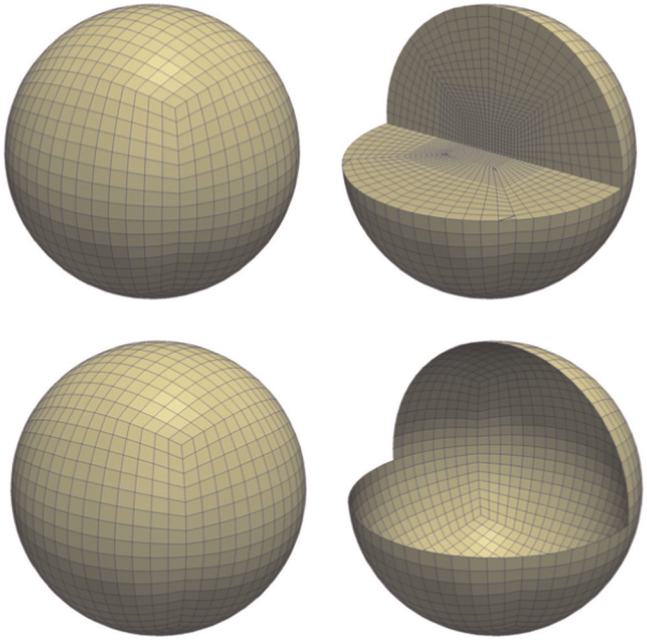

Fig. 1. An example illustrating how the surface triangulation (bottom row) is naturally induced by the volume or bulk (top row) triangulation. Part of the domain has been cut away and shown on the right to reveal some internal mesh structure [21].

Table 1
Parameter values for the coupled system of bulk-surface reaction–diffusion equations (2.1)–(2.6).

a	b	d	α_1	α_2	β_1	β_2	κ_1	κ_2
0.1	0.9	100	5/12	5	5/12	0	0	5

Table 2
Model parameter values used in simulations for Figs. 2–9.

Figure	d_Ω	d_Γ
2	1.0	1.0
3	1.0	10.0
5	1.0	20.0
6	10.0	1.0
7	10.0	10.0
8	20.0	10.0
9	20.0	20.0

the tangent plane, thus $\nabla_\Gamma u \cdot \boldsymbol{n} = 0$. The Laplace–Beltrami operator on the surface Γ is defined to be the tangential divergence of the tangential gradient $\Delta_\Gamma u = \nabla_\Gamma \cdot \nabla_\Gamma u$. For a vector function $\boldsymbol{u} = (u_1, u_2, \ldots, u_{N+1}) \in \mathbb{R}^{N+1}$ the tangential divergence is defined by

$$\nabla_\Gamma \cdot \boldsymbol{u} = \nabla \cdot \boldsymbol{u} - \sum_{i=1}^{N+1} (\nabla u_i \cdot \boldsymbol{n}) n_i.$$

2.2. A coupled system of bulk-surface reaction–diffusion equations (BSRDEs)

For a bounded volume $\Omega \subset \mathbb{R}^N$ $(N = 2, 3)$ with boundary $\Gamma := \partial\Omega$ and $I = [0, T]$ $(T > 0)$, let us assume that $u(\boldsymbol{x}, t)$, $v(\boldsymbol{x}, t) : \Omega \longrightarrow \mathbb{R}$ are two chemical concentrations (species) that react and diffuse in Ω and $r(\boldsymbol{x}, t)$, $s(\boldsymbol{x}, t) : \Gamma \longrightarrow \mathbb{R}$ be two chemical species residing only on the surface Γ which react and diffuse on the bulk surface. In the absence of cross-diffusion and assuming that coupling is only through the reaction kinetics, we pose the following non-dimensionalised coupled system of BSRDEs [21]:

$$\begin{cases} \begin{cases} u_t = \nabla^2 u + \gamma_\Omega f(u, v), \\ v_t = d_\Omega \nabla^2 v + \gamma_\Omega g(u, v), \end{cases} & \boldsymbol{x} \text{ on } \Omega, \ t > 0, \\ \begin{cases} r_t = \nabla_\Gamma^2 r + \gamma_\Gamma (f(r, s) - h_1(u, v, r, s)), \\ s_t = d_\Gamma \nabla_\Gamma^2 s + \gamma_\Gamma (g(r, s) - h_2(u, v, r, s)), \end{cases} & \boldsymbol{x} \text{ on } \Gamma, \ t > 0, \end{cases} \tag{2.1}$$

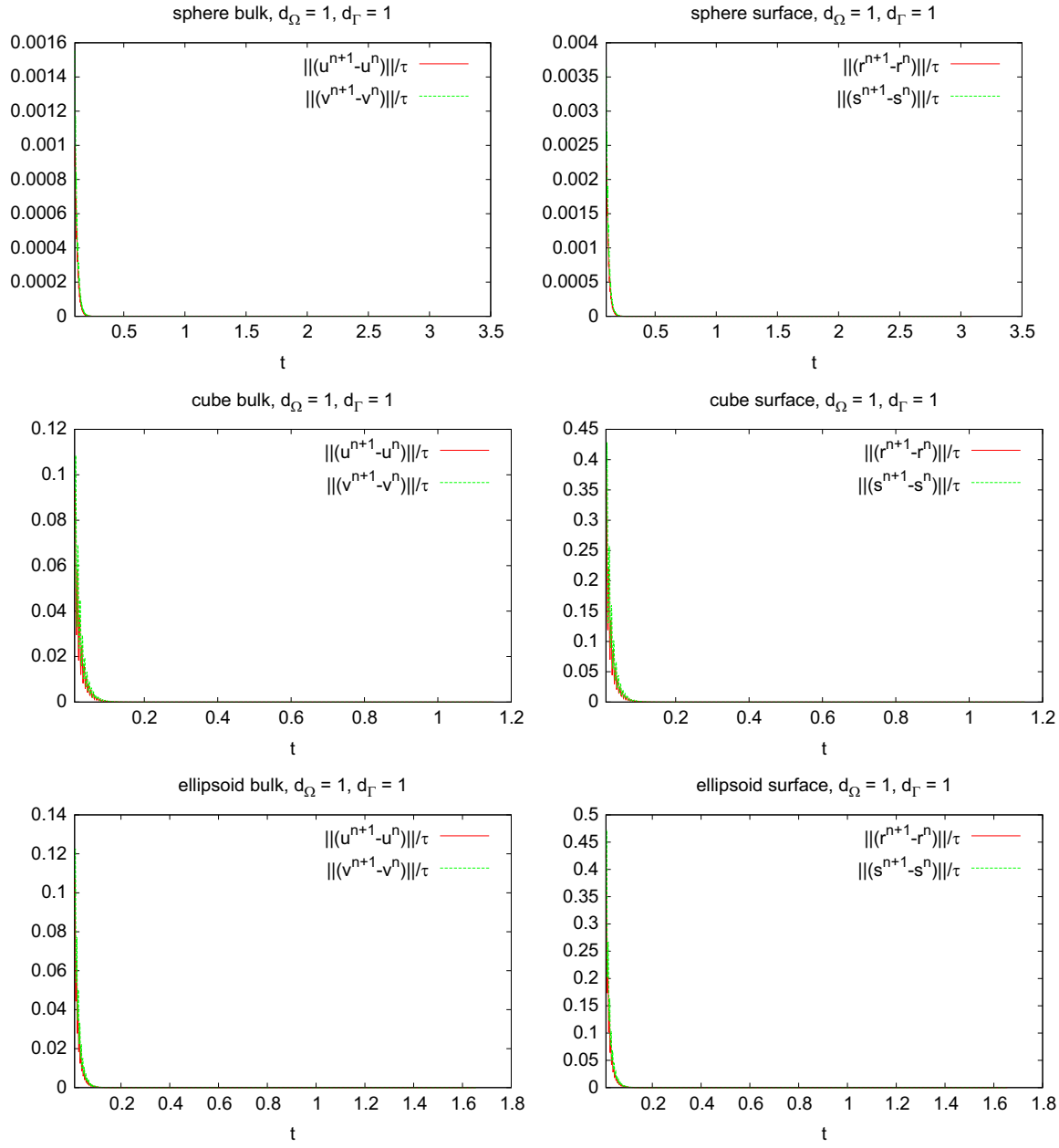

Fig. 2. Plots of the convergence graphs corresponding to the chemical species u and v in the bulk (left column) and r and s on the surface (right column) corresponding to the coupled system of BSRDEs (2.1)–(2.6) with $d_\Omega = 1$ in the bulk, $d_\Gamma = 1$ on the surface and $\gamma_\Omega = \gamma_\Gamma = 500$. The convergence criteria are defined by (4.1). Here we observe a rapid decay in the L_2-norm errors for the bulk and surface species respectively. There are no excitable wavenumbers to induce patterns and hence we do not observe exponential growth associated with growing wavenumbers to induce patterns. The uniform steady state is the only stable solution for the coupled system of BSRDEs (2.1)–(2.6). The evolution profile is independent of the geometry; the sphere, cube and ellipsoid all give similar evolution profiles (results not shown).

with coupling boundary conditions

$$\begin{cases} \dfrac{\partial u}{\partial \boldsymbol{\nu}} = \gamma_\Gamma h_1(u,v,r,s), \\ d_\Omega \dfrac{\partial v}{\partial \boldsymbol{\nu}} = \gamma_\Gamma h_2(u,v,r,s), \end{cases} \quad \boldsymbol{x} \text{ on } \Gamma,\ t>0. \tag{2.2}$$

In the above, $\nabla^2 = \frac{\partial^2}{\partial x^2}+\frac{\partial^2}{\partial y^2}+\frac{\partial^2}{\partial z^2}$ represents the Laplacian operator while ∇_Γ^2 denotes the Laplace–Beltrami operator, defined as the tangential divergence of the tangential gradient. $\boldsymbol{\nu}$ represents the outward pointing normal to the surface. d_Ω and d_Γ are positive diffusion coefficients in the bulk and on the surface respectively, representing the ratio between u and v, and r and s, respectively. γ_Ω and γ_Γ represent the length scale parameters in the bulk and on the surface respectively. In this formulation, we assume that $f(\cdot,\cdot)$ and $g(\cdot,\cdot)$ are nonlinear reaction kinetics in the bulk and on the surface. $h_1(u,v,r,s)$ and $h_2(u,v,r,s)$ are reactions representing the coupling of internal dynamics in the bulk Ω to the surface dynamics on the surface Γ. As a first attempt, we will consider a more generalised form of linear coupling of the following nature [18]:

$$h_1(u,v,r,s) = \alpha_1 r - \beta_1 u - \kappa_1 v, \tag{2.3}$$

$$h_2(u,v,r,s) = \alpha_2 s - \beta_2 u - \kappa_2 v, \tag{2.4}$$

where α_1, α_2, β_1, β_2, κ_1 and κ_2 are constant non-dimensionalised parameters. Initial conditions are given by the positive bounded functions $u_0(\boldsymbol{x})$, $v_0(\boldsymbol{x})$, $r_0(\boldsymbol{x})$ and $s_0(\boldsymbol{x})$.

2.2.1. Activator-depleted reaction kinetics: an illustrative example

From now onwards, we restrict our studies to the well-known *activator-depleted* substrate reaction model [10,25,28] also known as the Brusselator given by

$$f(u,v) = a - u + u^2 v, \tag{2.5}$$

$$g(u,v) = b - u^2 v, \tag{2.6}$$

where a and b are positive parameters. For analytical simplicity, we postulate the model system (2.7) in a more compact form given by

$$\begin{cases} \begin{cases} u_t = \nabla^2 u + f_1(u,v,r,s), \\ v_t = d_\Omega \nabla^2 v + f_2(u,v,r,s), \end{cases} & \boldsymbol{x} \text{ on } \Omega,\ t>0, \\ \begin{cases} r_t = \nabla_\Gamma^2 r + f_3(u,v,r,s), \\ s_t = d_\Gamma \nabla_\Gamma^2 s + f_4(u,v,r,s), \end{cases} & \boldsymbol{x} \text{ on } \Gamma,\ t>0, \end{cases} \tag{2.7}$$

with coupling boundary conditions (2.2). In the above, we have defined appropriately

$$f_1(u,v,r,s) = \gamma_\Omega(a - u + u^2 v), \tag{2.8}$$

$$f_2(u,v,r,s) = \gamma_\Omega(b - u^2 v), \tag{2.9}$$

$$f_3(u,v,r,s) = \gamma_\Gamma\left(a - r + r^2 s - \alpha_1 r + \beta_1 u + \kappa_1 v\right), \tag{2.10}$$

$$f_4(u,v,r,s) = \gamma_\Gamma\left(b - r^2 s - \alpha_2 s + \beta_2 u + \kappa_2 v\right). \tag{2.11}$$

2.3. Applications

Applications of reaction–diffusion systems are abundant in the literature and these include (but not limited to) modelling pattern formation in developmental biology, molecular dynamics in cell motility, borne and tissue regeneration in biomedical engineering and fluid–structure interactions in fluid dynamics [13]. Specific examples are given by models describing the growth of an epitaxial layer and dendritic in developmental biology [2], GTPase molecular dynamics in cell motility [15] and soluble surfactants in fluid dynamics [3].

2.4. Uniform steady states

Definition 2.1 (*Uniform steady state*). A point (u^*, v^*, r^*, s^*) is a uniform steady state of the coupled system of BSRDEs (2.7) with reaction kinetics (2.5)–(2.6) if it solves the nonlinear algebraic system given by

$$f_i(u^*, v^*, r^*, s^*) = 0 \quad \text{for all } i = 1,2,3,4,$$

and satisfies the boundary conditions given by (2.2).

Theorem 2.1 (*Existence and uniqueness of the uniform steady state*). *The coupled system of BSRDEs (2.7) with boundary conditions (2.2) admits a unique steady state given by*

$$(u^*, v^*, r^*, s^*) = \left(a+b, \frac{b}{(a+b)^2}, a+b, \frac{b}{(a+b)^2}\right), \tag{2.12}$$

provided the compatibility condition on the coefficients of the coupling is satisfied:

$$(\beta_1 - \alpha_1)(\kappa_2 - \alpha_2) - \kappa_1 \beta_2 = 0. \tag{2.13}$$

Proof. For proof see Madzvamuse et al. [21].□

Remark 2.1. The conditions for *diffusion-driven* instability for the coupled system were derived and proved in [21].

Remark 2.2. The compatibility condition (2.13) will be used to select the parameters associated with the boundary conditions.

3. The bulk-surface finite element method for reaction–diffusion systems on stationary volumes

In the following we present two sets of results. We use the finite element method to discretise in space with piecewise bilinear elements, and the implicit second order fractional-step θ scheme to discretise in time using the Newton method to solve the non-linearities [20].

3.1. Weak variational form

Let $\varphi \in H^1(\Omega)$ and $\psi \in H^1(\Gamma)$. Then, multiplying (2.7) by φ and ψ, we seek $u, v \in L^2(0,t;H^1(\Omega))$ and $r, s \in L^2(0,t;H^1(\Gamma))$, such that

$$\begin{cases} \begin{cases} \int_\Omega (u_t\varphi + \nabla u \cdot \nabla\varphi) \\ \quad = \gamma_\Omega \int_\Omega (a - u + u^2 v)\varphi + \gamma_\Gamma \int_\Gamma (\alpha_1 r - \beta_1 u - \kappa_1 v)\varphi, \\ \int_\Omega (v_t\varphi + d_\Omega \nabla v \cdot \nabla\varphi) \\ \quad = \gamma_\Omega \int_\Omega (b - u^2 v)\varphi + \gamma_\Gamma \int_\Gamma (\alpha_2 s - \beta_2 u - \kappa_2 v)\varphi, \end{cases} & \boldsymbol{x} \text{ on } \Omega,\ t>0, \\ \begin{cases} \int_\Gamma (r_t\psi + \nabla_\Gamma r \cdot \nabla_\Gamma \psi) \\ \quad = \gamma_\Gamma \int_\Gamma (a - r + r^2 s - \alpha_1 r + \beta_1 u + \kappa_1 v)\psi, \\ \int_\Gamma (s_t\psi + d_\Gamma \nabla_\Gamma s \cdot \nabla_\Gamma \psi) \\ \quad = \gamma_\Gamma \int_\Gamma (b - r^2 s - \alpha_2 s + \beta_2 u + \kappa_2 v)\psi, \end{cases} & \boldsymbol{x} \text{ on } \Gamma,\ t>0. \end{cases} \tag{3.1}$$

In the above, we have used Green's identities with the boundary conditions (2.2) to obtain the boundary integrals.

3.2. Spatial discretisation

Let $\Omega_h \subset \Omega$ and $\Gamma_h \subset \Gamma$ be discretisations of the original domains with N_Ω and N_Γ vertices respectively. Let us take the finite dimensional subspaces $V_{\Omega_h} \subset H^1(\Omega)$ and $V_{\Gamma_h} \subset H^1(\Gamma)$. Then, we seek $u_h, v_h \in L^2(0,t;V_{\Omega_h})$ and $r_h, s_h \in L^2(0,t;V_{\Gamma_h})$ such that for all

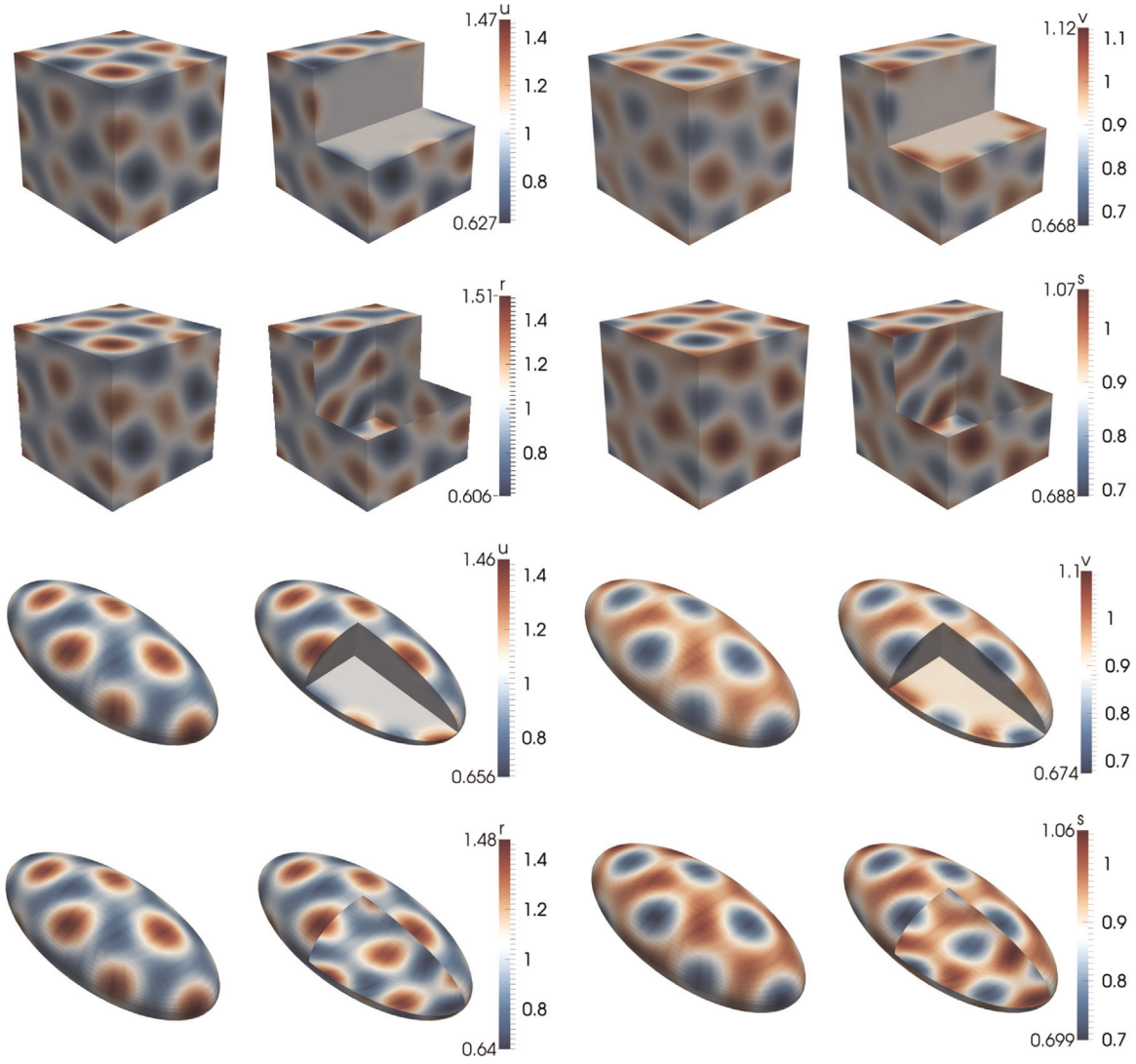

Fig. 3. Numerical solutions corresponding to the coupled system of BSRDEs (2.1)–(2.6) with $d_\Omega = 1$ in the bulk, $d_\Gamma = 10$ on the surface and $\gamma_\Omega = \gamma_\Gamma = 500$. The surface reaction–diffusion system induces patterning in a small band close to the surface. In the bulk, no patterns form almost everywhere. The patterning behaviour is independent of the geometry. Rows 1 and 3: solutions in the bulk representing u and v. Rows 2 and 4: solutions on the surface representing r and s. Second and fourth columns represent cross sections of the bulk and the surface respectively.

$\varphi_h \in V_{\Omega_h}$ and $\psi_h \in V_{\Gamma_h}$

$$\begin{cases} \begin{cases} \int_{\Omega_h}(u_{h,t}\varphi_h + \nabla u_h \cdot \nabla\varphi_h) \\ \quad = \gamma_\Omega \int_{\Omega_h}(a - u_h + u_h^2 v_h)\varphi_h + \gamma_\Gamma \int_{\Gamma_h}(\alpha_1 r_h - \beta_1 u_h - \kappa_1 v_h)\varphi_h, \\ \int_{\Omega_h}(v_{h,t}\varphi_h + d_\Omega \nabla v_h \cdot \nabla\varphi_h) \\ \quad = \gamma_\Omega \int_{\Omega_h}(b - u_h^2 v_h)\varphi_h + \gamma_\Gamma \int_{\Gamma_h}(\alpha_2 s_h - \beta_2 u_h - \kappa_2 v_h)\varphi_h, \end{cases} & \boldsymbol{x} \text{ on } \Omega_h,\ t > 0, \\ \begin{cases} \int_{\Gamma_h}(r_{h,t}\psi_h + \nabla_\Gamma r_h \cdot \nabla_\Gamma \psi_h) \\ \quad = \gamma_\Gamma \int_{\Gamma_h}(a - r_h + r_h^2 s_h - \alpha_1 r_h + \beta_1 u_h + \kappa_1 v_h)\psi_h, \\ \int_{\Gamma_h}(s_{h,t}\psi_h + d_\Gamma \nabla_\Gamma s_h \cdot \nabla_\Gamma \psi_h) \\ \quad = \gamma_\Gamma \int_{\Gamma_h}(b - r_h^2 s_h - \alpha_2 s_h + \beta_2 u_h + \kappa_2 v_h)\psi_h, \end{cases} & \boldsymbol{x} \text{ on } \Gamma_h,\ t > 0. \end{cases}$$

Let $\{\varphi_i\}_{i=1}^{N_\Omega}$ and $\{\psi_i\}_{i=1}^{N_\Gamma}$ be two set of piecewise bilinear shape functions on Ω_h and Γ_h respectively. Then these sets form a basis of V_Ω and V_Γ. Thus, we can write the discrete solution variables as $u_h = \sum_{i=1}^{N_\Omega} u_i\varphi_i := \boldsymbol{u}\cdot\boldsymbol{\varphi}$, and similarly for the other variables. Then, the above can be written compactly in matrix form as

$$\begin{cases} \begin{cases} M_{\boldsymbol{\varphi}}\boldsymbol{u}_t + \gamma_\Omega M_{\boldsymbol{\varphi}}\boldsymbol{u} + A_{\boldsymbol{\varphi}}\boldsymbol{u} - \gamma_\Omega B_{\boldsymbol{\varphi}}(\boldsymbol{u},\boldsymbol{v})\boldsymbol{u} \\ \quad - \gamma_\Gamma(\alpha_1 M_{\varphi\psi}\boldsymbol{r} - \beta_1 M_{\varphi\varphi}\boldsymbol{u} - \kappa_1 M_{\varphi\varphi}\boldsymbol{v}) = \gamma_\Omega a\mathbb{1}_{\boldsymbol{\varphi}}, \\ M_{\boldsymbol{\varphi}}\boldsymbol{v}_t + d_\Omega A_{\boldsymbol{\varphi}}\boldsymbol{v} + \gamma_\Omega B_{\boldsymbol{\varphi}}(\boldsymbol{u},\boldsymbol{u})\boldsymbol{v} \\ \quad - \gamma_\Gamma(\alpha_2 M_{\varphi\psi}\boldsymbol{s} - \beta_2 M_{\varphi\varphi}\boldsymbol{u} - \kappa_2 M_{\varphi\varphi}\boldsymbol{v}) = \gamma_\Omega b\mathbb{1}_{\boldsymbol{\varphi}}, \end{cases} & \text{in } \Omega_h \times (0,T \\ \begin{cases} M_{\boldsymbol{\psi}}\boldsymbol{r}_t + \gamma_\Gamma M_{\boldsymbol{\psi}}\boldsymbol{r} + A_{\boldsymbol{\psi}}\boldsymbol{r} - \gamma_\Gamma B_{\boldsymbol{\psi}}(\boldsymbol{r},\boldsymbol{s})\boldsymbol{r} \\ \quad + \gamma_\Gamma(\alpha_1 M_{\psi\psi}\boldsymbol{r} - \beta_1 M_{\psi\varphi}\boldsymbol{u} - \kappa_1 M_{\psi\varphi}\boldsymbol{v}) = \gamma_\Gamma a\mathbb{1}_{\boldsymbol{\psi}}, \\ M_{\boldsymbol{\psi}}\boldsymbol{s}_t + d_\Gamma A_{\boldsymbol{\psi}}\boldsymbol{s} + \gamma_\Gamma B_{\boldsymbol{\psi}}(\boldsymbol{r},\boldsymbol{r})\boldsymbol{s} \\ \quad + \gamma_\Gamma(\alpha_2 M_{\psi\psi}\boldsymbol{s} - \beta_2 M_{\psi\varphi}\boldsymbol{u} - \kappa_2 M_{\psi\varphi}\boldsymbol{v}) = \gamma_\Gamma b\mathbb{1}_{\boldsymbol{\psi}}, \end{cases} & \text{.on } \Gamma_h \times (0,T], \end{cases} \tag{3.2}$$

where $A_{\boldsymbol{\varphi}}$ and $M_{\boldsymbol{\varphi}}$ are the stiffness and mass matrices respectively with entries

$$(A_{\boldsymbol{\varphi}})_{ij} = \int_{\Omega_h} \nabla\varphi_i \cdot \nabla\varphi_j \, d\boldsymbol{x} \quad \text{and} \quad (M_{\boldsymbol{\varphi}})_{ij} = \int_{\Omega_h} \varphi_i\varphi_j \, d\boldsymbol{x}. \tag{3.3}$$

$\mathbb{1}_\varphi$ is the column vector with j-th entry $\int_{\Omega_h}\varphi_j$. Given some vectors $\boldsymbol{a}$, $\boldsymbol{b}$ and $\boldsymbol{c}$, $B_{\boldsymbol{\varphi}}(\boldsymbol{a},\boldsymbol{b})$ is the matrix with entries

$$(B_{\boldsymbol{\varphi}})_{ij}=\int_{\Omega_h}(\boldsymbol{a}\cdot\varphi)(\boldsymbol{b}\cdot\varphi)\varphi_i\varphi_j\,d\boldsymbol{x}. \tag{3.4}$$

Similar quantities are defined for $A_{\boldsymbol{\psi}}$, $M_{\boldsymbol{\psi}}$, $\mathbb{1}_\psi$ and $B_{\boldsymbol{\psi}}$. The matrices $M_{\varphi\varphi}$, $M_{\varphi\psi}$, $M_{\psi\varphi}$ and $M_{\psi\psi}$ have entries

$$(M_{\varphi\varphi})_{ij}=\int_{\Gamma_h}\varphi_i\varphi_j\,d\boldsymbol{x},\quad (M_{\varphi\psi})_{ij}=\int_{\Gamma_h}\varphi_i\psi_j\,d\boldsymbol{x},$$
$$(M_{\psi\varphi})_{ij}=\int_{\Gamma_h}\psi_i\varphi_j\,d\boldsymbol{x}\quad\text{and}\quad(M_{\psi\psi})_{ij}=\int_{\Gamma_h}\psi_i\psi_j\,d\boldsymbol{x}.$$

3.2.1. Mesh generation

For finite element methods involving bulk and surface coupled dynamics, it is natural to define the surface triangulation as a collection of the faces of the elements of the bulk triangulation whose vertices lie on the surface. This implies that the surface triangulation is the trace of the bulk triangulation [17]. First we approximate Ω by Ω_h a bulk triangulation. Next we construct Γ_h to be the triangulation of the surface geometry Γ by defining $\Gamma_h=\Omega_h|_{\partial\Omega_h}$, i.e. the vertices of Γ_h are the same as those lying on the surface of Ω_h. In particular, then, we have $\partial\Omega_h=\Gamma_h$. An example mesh is shown in Fig. 1 [21]. The bulk triangulation induces the surface triangulation as illustrated. Throughout, we use hexahedral meshes for the bulk geometries which induce quadrilateral meshes for the surface geometries. For further details on techniques for generating bulk and surface triangulations with adaptivity, the reader is referred to the work of Köster et al. [17].

3.3. Time discretisation

We carry out the time-discretisation using the fractional-step θ method. This method is second order accurate when choosing $\theta=1-1/\sqrt{2}$ and was the quickest in a selection of tested methods in a previous investigation [20]. For convergence, stability and performance of the numerical method, the reader is referred to [20]. For the time discretisation let T_m denote the maximum time of interest, τ denote the time step and J be a fixed nonnegative integer, then

$$\tau=\frac{T_m}{J}\quad\text{and}\quad t_k=k\tau,\quad k=0,1,2,\ldots,J.$$

We denote the approximate solution at time t_k by $u_h^k=u_h(\cdot,t_k)=\boldsymbol{u}^k\cdot\varphi$ and similarly for the other variables. Following from (3.2), the fractional-step θ method is implemented as follows: Starting with the previous solution $(\boldsymbol{u}^n,\boldsymbol{v}^n,\boldsymbol{r}^n,\boldsymbol{s}^n)$, we first solve for the

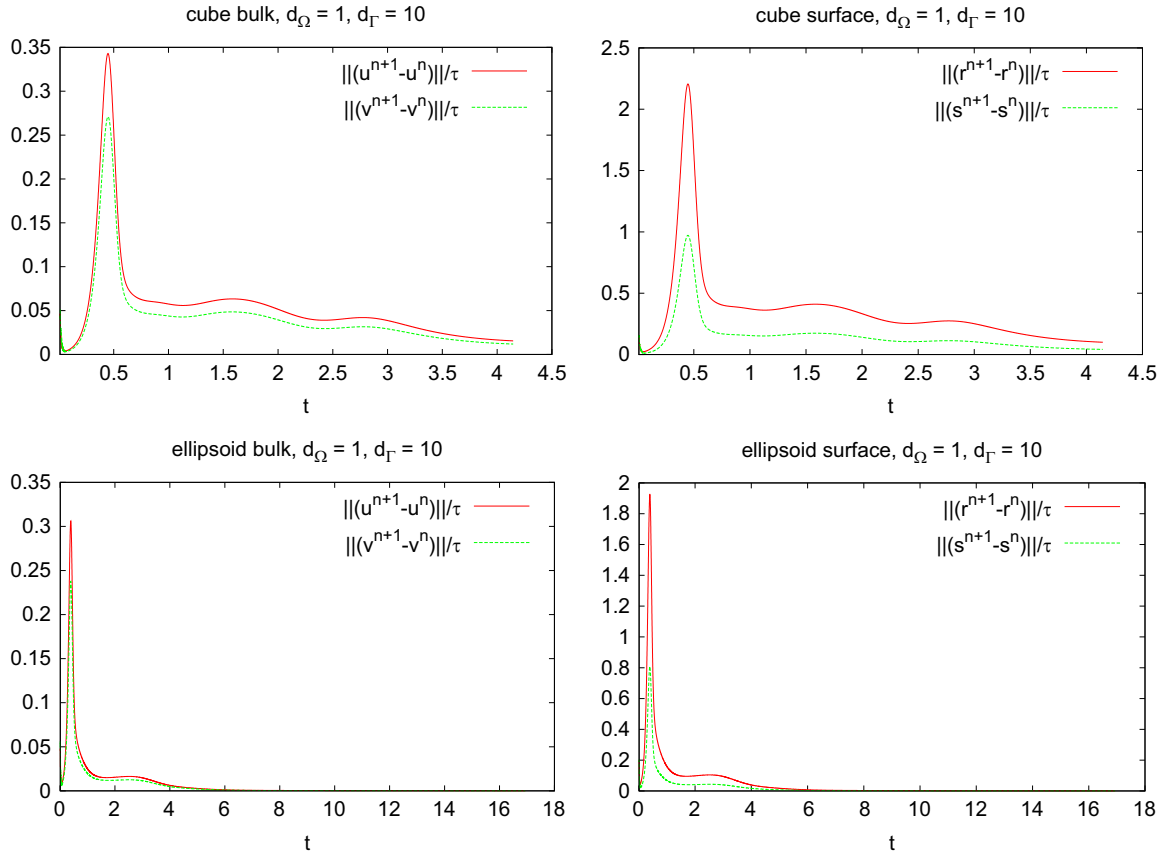

Fig. 4. Plots of the convergence graphs corresponding to the chemical species u and v in the bulk (left column) and r and s on the surface (right column) corresponding to the coupled system of BSRDEs (2.1)–(2.6) with $d_\Omega=1$ in the bulk, $d_\Gamma=10$ on the surface and $\gamma_\Omega=\gamma_\Gamma=500$. The convergence criteria are defined by (4.1). The evolution of the L_2-norm errors is characterised by three key phases: (i) an initial rapid decay due to the smoothing effects of diffusion (ii) an intermediate stage characterised by an exponential growth of the positive excitable wavenumbers to induce the formation of spatial structure. It is during this phase that the uniform steady state is driven unstable, and (iii) a final stage where nonlinear terms become dominant and act as bounds to the exponentially growing modes resulting in the formation of a spatially stable inhomogeneous state corresponding to the coupled system of BSRDEs (2.1)–(2.6).

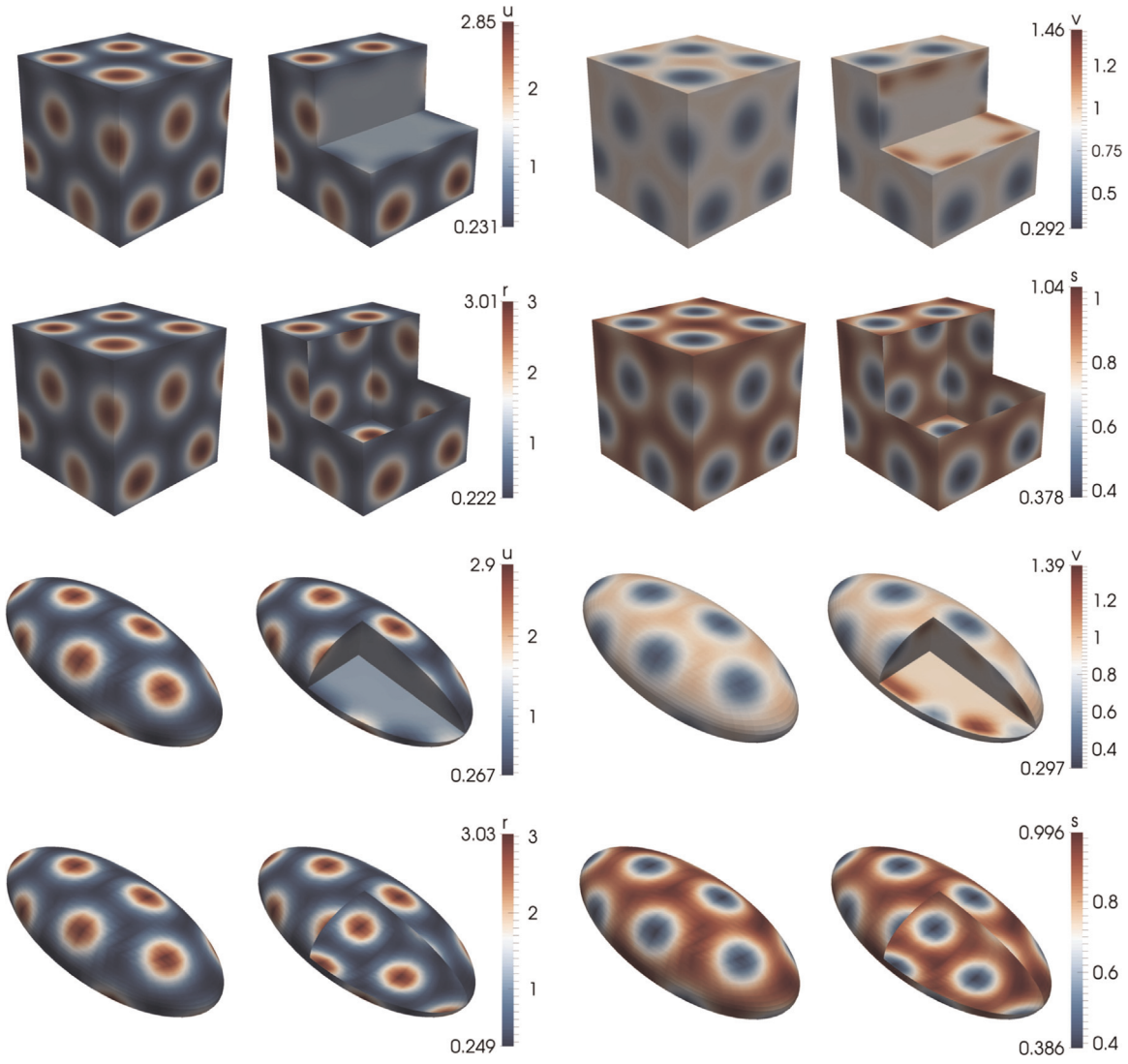

Fig. 5. Numerical solutions corresponding to the coupled system of BSRDEs (2.1)–(2.6) with $d_\Omega = 1$ in the bulk, $d_\Gamma = 20$ on the surface and $\gamma_\Omega = \gamma_\Gamma = 500$. The pattering process is similar to that shown in Fig. 3 for large values of d_Γ. Rows 2 and 4: solutions on the surface representing r and s. Second and fourth columns represent cross sections of the bulk and the surface respectively.

intermediate solution $(\boldsymbol{u}^{n+\theta}, \boldsymbol{v}^{n+\theta}, \boldsymbol{r}^{n+\theta}, \boldsymbol{s}^{n+\theta})$

$$
\begin{cases}
M_\varphi \dfrac{\boldsymbol{u}^{n+\theta}-\boldsymbol{u}^{n}}{\theta\tau} + A_\varphi \boldsymbol{u}^{n+\theta} + \gamma_\Omega M_\varphi \boldsymbol{u}^{n+\theta} \\
\quad -\gamma_\Gamma(\alpha_1 M_{\varphi\psi}\boldsymbol{r}^{n+\theta} - \beta_1 M_{\varphi\varphi}\boldsymbol{u}^{n+\theta} - \kappa_1 M_{\varphi\varphi}\boldsymbol{v}^{n+\theta}) = \gamma_\Omega a\mathbb{1}_\varphi + \gamma_\Omega B_\varphi(\boldsymbol{u}^n, \boldsymbol{v}^n)\boldsymbol{u}^n, \\
M_\varphi \dfrac{\boldsymbol{v}^{n+\theta}-\boldsymbol{v}^{n}}{\theta\tau} + d_\Omega A_\varphi \boldsymbol{v}^{n+\theta} \\
\quad -\gamma_\Gamma(\alpha_2 M_{\varphi\psi}\boldsymbol{s}^{n+\theta} - \beta_2 M_{\varphi\varphi}\boldsymbol{u}^{n+\theta} - \kappa_2 M_{\varphi\varphi}\boldsymbol{v}^{n+\theta}) = \gamma_\Omega b\mathbb{1}_\varphi - \gamma_\Omega B_\varphi(\boldsymbol{u}^n, \boldsymbol{u}^n)\boldsymbol{v}^n, \\
M_\psi \dfrac{\boldsymbol{r}^{n+\theta}-\boldsymbol{r}^{n}}{\theta\tau} + A_\psi \boldsymbol{r}^{n+\theta} + \gamma_\Gamma M_\psi \boldsymbol{r}^{n+\theta} \\
\quad +\gamma_\Gamma(\alpha_1 M_{\psi\psi}\boldsymbol{r}^{n+\theta} - \beta_1 M_{\psi\varphi}\boldsymbol{u}^{n+\theta} - \kappa_1 M_{\psi\varphi}\boldsymbol{v}^{n+\theta}) = \gamma_\Gamma a\mathbb{1}_\psi + \gamma_\Gamma B_\psi(\boldsymbol{r}^n, \boldsymbol{s}^n)\boldsymbol{r}^n, \\
M_\psi \dfrac{\boldsymbol{s}^{n+\theta}-\boldsymbol{s}^{n}}{\theta\tau} + d_\Gamma A_\psi \boldsymbol{s}^{n+\theta} \\
\quad +\gamma_\Gamma(\alpha_2 M_{\psi\psi}\boldsymbol{s}^{n+\theta} - \beta_2 M_{\psi\varphi}\boldsymbol{u}^{n+\theta} - \kappa_2 M_{\psi\varphi}\boldsymbol{v}^{n+\theta}) = \gamma_\Gamma b\mathbb{1}_\psi - \gamma_\Gamma B_\psi(\boldsymbol{r}^n, \boldsymbol{r}^n)\boldsymbol{s}^n,
\end{cases}
$$

then for the second intermediate solution $(\boldsymbol{u}^{n+1-\theta}, \boldsymbol{v}^{n+1-\theta}, \boldsymbol{r}^{n+1-\theta}, \boldsymbol{s}^{n+1-\theta})$ we solve

$$
\begin{cases}
M_\varphi \dfrac{\boldsymbol{u}^{n+1-\theta}-\boldsymbol{u}^{n+\theta}}{(1-2\theta)\tau} - \gamma_\Omega B_\varphi(\boldsymbol{u}^{n+1-\theta}, \boldsymbol{v}^{n+1-\theta})\boldsymbol{u}^{n+1-\theta} = \gamma_\Omega a\mathbb{1}_\varphi \\
\quad -A_\varphi \boldsymbol{u}^{n+\theta} - \gamma_\Omega M_\varphi \boldsymbol{u}^{n+\theta} + \gamma_\Gamma(\alpha_1 M_{\varphi\psi}\boldsymbol{r}^{n+\theta} - \beta_1 M_{\varphi\varphi}\boldsymbol{u}^{n+\theta} - \kappa_1 M_{\varphi\varphi}\boldsymbol{v}^{n+\theta}) \\
M_\varphi \dfrac{\boldsymbol{v}^{n+1-\theta}-\boldsymbol{v}^{n+\theta}}{(1-2\theta)\tau} + \gamma_\Omega B_\varphi(\boldsymbol{u}^{n+1-\theta}, \boldsymbol{u}^{n+1-\theta})\boldsymbol{v}^{n+1-\theta} = \gamma_\Omega b\mathbb{1}_\varphi \\
\quad -d_\Omega A_\varphi \boldsymbol{v}^{n+\theta} + \gamma_\Gamma(\alpha_2 M_{\varphi\psi}\boldsymbol{s}^{n+\theta} - \beta_2 M_{\varphi\varphi}\boldsymbol{u}^{n+\theta} - \kappa_2 M_{\varphi\varphi}\boldsymbol{v}^{n+\theta}), \\
M_\psi \dfrac{\boldsymbol{r}^{n+1-\theta}-\boldsymbol{r}^{n+\theta}}{(1-2\theta)\tau} - \gamma_\Gamma B_\psi(\boldsymbol{r}^{n+1-\theta}, \boldsymbol{s}^{n+1-\theta})\boldsymbol{r}^{n+1-\theta} = \gamma_\Gamma a\mathbb{1}_\psi \\
\quad -A_\psi \boldsymbol{r}^{n+\theta} - \gamma_\Gamma M_\psi \boldsymbol{r}^{n+\theta} - \gamma_\Gamma(\alpha_1 M_{\psi\psi}\boldsymbol{r}^{n+\theta} - \beta_1 M_{\psi\varphi}\boldsymbol{u}^{n+\theta} - \kappa_1 M_{\psi\varphi}\boldsymbol{v}^{n+\theta}), \\
M_\psi \dfrac{\boldsymbol{s}^{n+1-\theta}-\boldsymbol{s}^{n+\theta}}{(1-2\theta)\tau} + \gamma_\Gamma B_\psi(\boldsymbol{r}^{n+1-\theta}, \boldsymbol{r}^{n+1-\theta})\boldsymbol{s}^{n+1-\theta} = \gamma_\Gamma b\mathbb{1}_\psi \\
\quad -d_\Gamma A_\psi \boldsymbol{s}^{n+\theta} - \gamma_\Gamma(\alpha_2 M_{\psi\psi}\boldsymbol{s}^{n+\theta} - \beta_2 M_{\psi\varphi}\boldsymbol{u}^{n+\theta} - \kappa_2 M_{\psi\varphi}\boldsymbol{v}^{n+\theta}),
\end{cases}
\tag{3.5}
$$

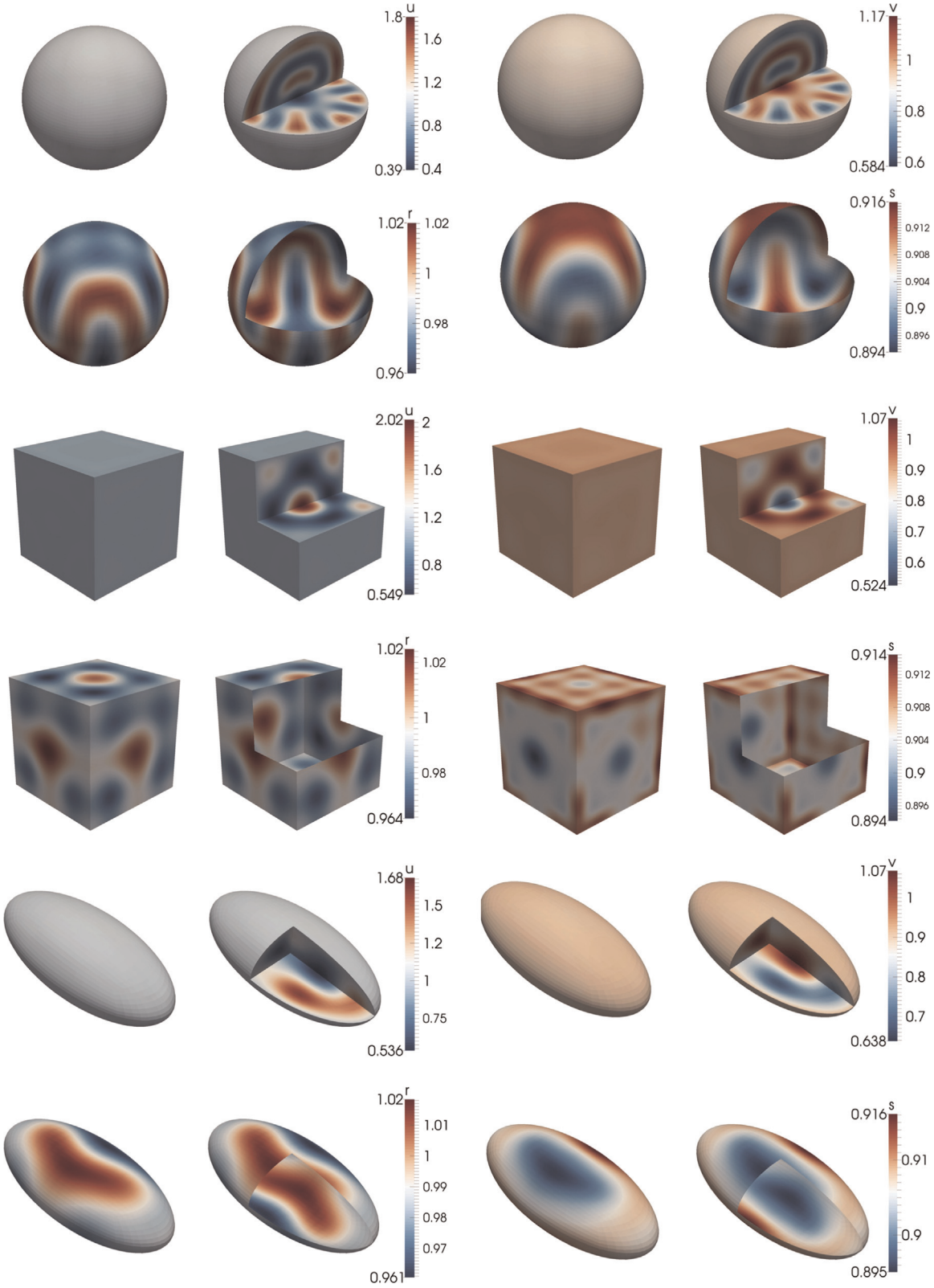

Fig. 6. Numerical solutions corresponding to the coupled system of BSRDEs (2.1)–(2.6) with $d_\Omega = 10$ in the bulk, $d_\Gamma = 1$ on the surface and $\gamma_\Omega = \gamma_\Gamma = 500$. The bulk reaction–diffusion system is able to induce patterning almost everywhere on the surface. Rows 2, 4 and 6: solutions on the surface representing r and s. Second and fourth columns represent cross sections of the bulk and the surface respectively.

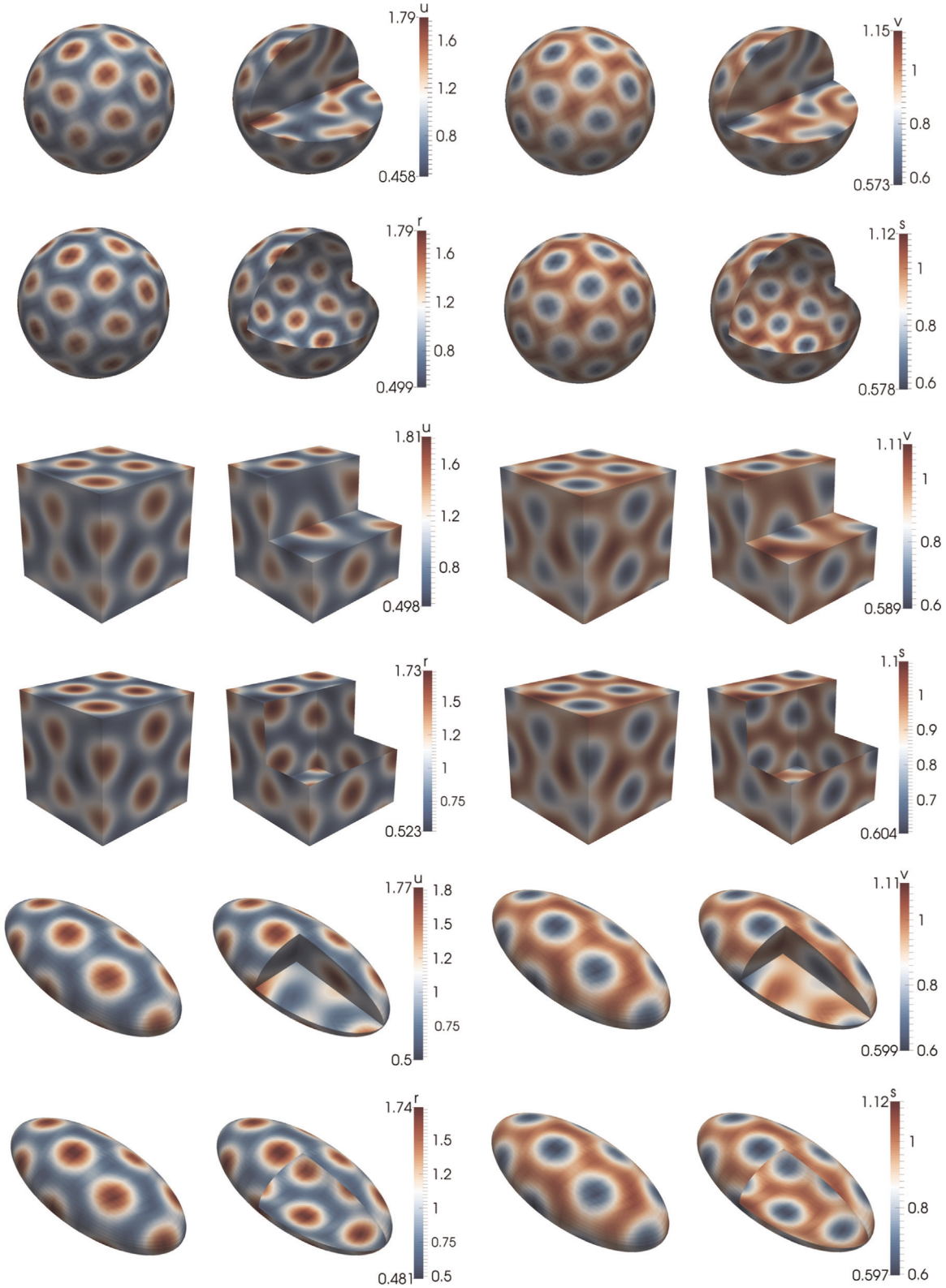

Fig. 7. Numerical solutions corresponding to the coupled system of BSRDEs (2.1)–(2.6) with $d_\Omega = 10$ in the bulk, $d_\Gamma = 10$ on the surface and $\gamma_\Omega = \gamma_\Gamma = 500$. The bulk and surface reaction–diffusion systems both have the capability to induce patterning. Rows 2, 4 and 6: solutions on the surface representing r and s. Second and fourth columns represent cross sections of the bulk and the surface respectively.

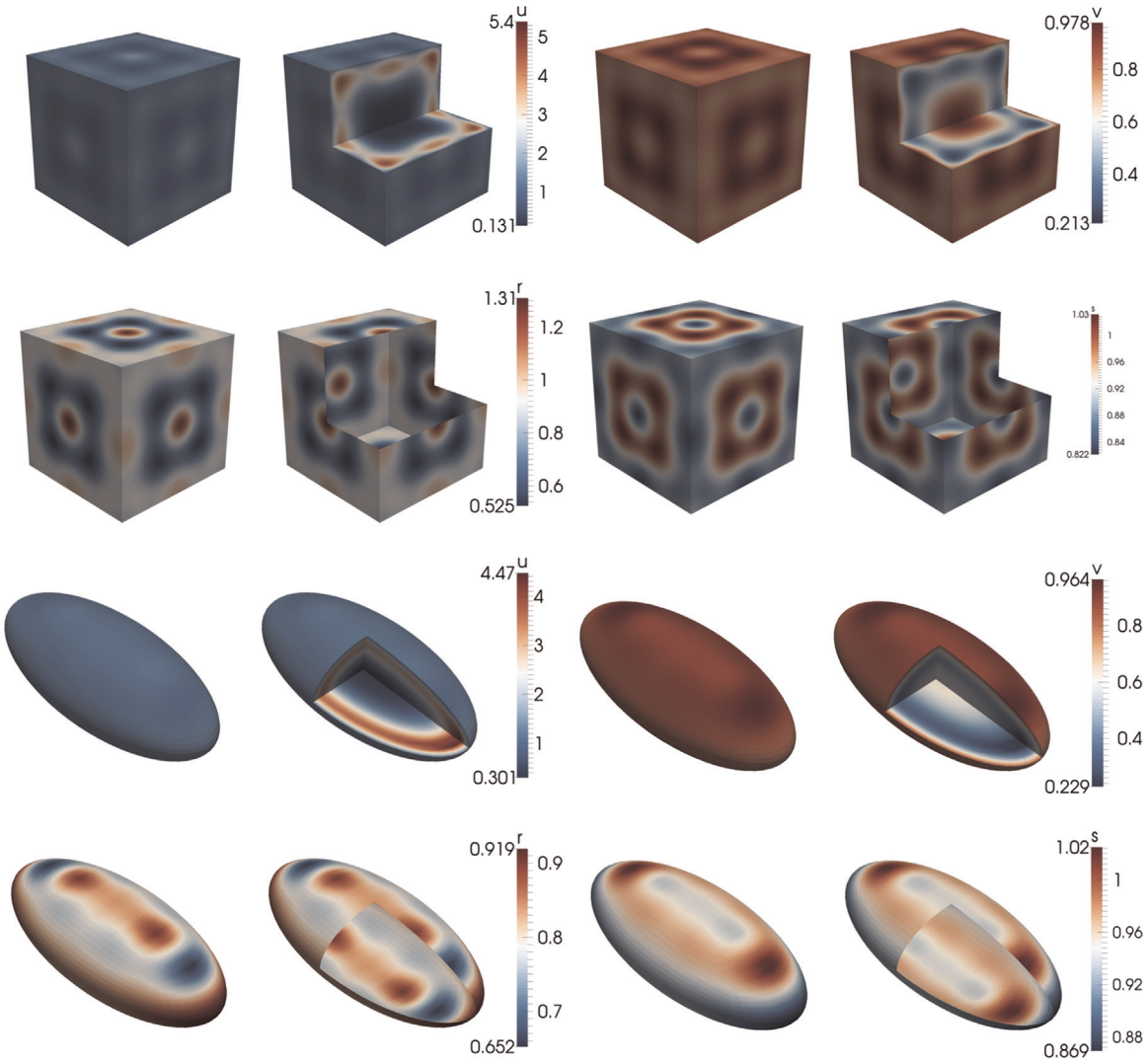

Fig. 8. Numerical solutions corresponding to the coupled system of BSRDEs (2.1)–(2.6) with $d_\Omega = 20$ in the bulk, $d_\Gamma = 10$ on the surface and $\gamma_\Omega = \gamma_\Gamma = 500$. The coupled system of BSRDEs induces pattering in the bulk and on the surface. Rows 2 and 4: solutions on the surface representing r and s. Second and fourth columns represent cross sections of the bulk and the surface respectively.

and finally for the new solution $(\boldsymbol{u}^{n+1}, \boldsymbol{v}^{n+1}, \boldsymbol{r}^{n+1}, \boldsymbol{s}^{n+1})$ we solve

$$
\begin{cases}
M_\varphi \dfrac{\boldsymbol{u}^{n+1} - \boldsymbol{u}^{n+1-\theta}}{\theta\tau} + A_\varphi \boldsymbol{u}^{n+1} + \gamma_\Omega M_\varphi \boldsymbol{u}^{n+1} \\
\quad - \gamma_\Gamma(\alpha_1 M_{\varphi\psi}\boldsymbol{r}^{n+1} - \beta_1 M_{\varphi\varphi}\boldsymbol{u}^{n+1} - \kappa_1 M_{\varphi\varphi}\boldsymbol{v}^{n+1}) \\
\quad = \gamma_\Omega a\mathbb{1}_\varphi + \gamma_\Omega B_\varphi(\boldsymbol{u}^{n+1-\theta}, \boldsymbol{v}^{n+1-\theta})\boldsymbol{u}^{n+1-\theta}, \\
M_\varphi \dfrac{\boldsymbol{v}^{n+1} - \boldsymbol{v}^{n+1-\theta}}{\theta\tau} + d_\Omega A_\varphi \boldsymbol{v}^{n+1} \\
\quad - \gamma_\Gamma(\alpha_2 M_{\varphi\psi}\boldsymbol{s}^{n+1} - \beta_2 M_{\varphi\varphi}\boldsymbol{u}^{n+1} - \kappa_2 M_{\varphi\varphi}\boldsymbol{v}^{n+1}) \\
\quad = \gamma_\Omega b\mathbb{1}_\varphi - \gamma_\Omega B_\varphi(\boldsymbol{u}^{n+1-\theta}, \boldsymbol{u}^{n+1-\theta})\boldsymbol{v}^{n+1-\theta}, \\
M_\psi \dfrac{\boldsymbol{r}^{n+1} - \boldsymbol{r}^{n+1-\theta}}{\theta\tau} + A_\psi \boldsymbol{r}^{n+1} + \gamma_\Gamma M_\psi \boldsymbol{r}^{n+1} \\
\quad + \gamma_\Gamma(\alpha_1 M_{\psi\psi}\boldsymbol{r}^{n+1} - \beta_1 M_{\psi\varphi}\boldsymbol{u}^{n+1} - \kappa_1 M_{\psi\varphi}\boldsymbol{v}^{n+1}) \\
\quad = \gamma_\Gamma a\mathbb{1}_\psi + \gamma_\Gamma B_\psi(\boldsymbol{r}^{n+1-\theta}, \boldsymbol{s}^{n+1-\theta})\boldsymbol{r}^{n+1-\theta}, \\
M_\psi \dfrac{\boldsymbol{s}^{n+1} - \boldsymbol{s}^{n+1-\theta}}{\theta\tau} + d_\Gamma A_\psi \boldsymbol{s}^{n+1} \\
\quad + \gamma_\Gamma(\alpha_2 M_{\psi\psi}\boldsymbol{s}^{n+1} - \beta_2 M_{\psi\varphi}\boldsymbol{u}^{n+1} - \kappa_2 M_{\psi\varphi}\boldsymbol{v}^{n+1}) \\
\quad = \gamma_\Gamma b\mathbb{1}_\psi - \gamma_\Gamma B_\psi(\boldsymbol{r}^{n+1-\theta}, \boldsymbol{r}^{n+1-\theta})\boldsymbol{s}^{n+1-\theta}.
\end{cases}
$$

The presence of the B matrices on the left-hand side make the system in the second step (3.5) nonlinear. The nonlinearities are solved using the iterative Newton method [20].

4. Numerical simulations of the coupled system of BSRDEs

For illustrative purposes let us take the parameter values shown in Table 1 which satisfy the compatibility condition (2.13). For these parameter values the unique equilibrium state is given by $(u^*, v^*, r^*, s^*) = (1, 0.9, 1, 0.9)$. We stop the simulations when the L_2-norm of the difference of the numerical solutions between two successive timesteps reaches some tolerance

$$
\frac{\|u_h^{n+1} - u_h^n\|}{\tau} := \frac{1}{\tau}\left(\int_\Omega (u_h^{n+1} - u_h^n)^2\right)^{1/2} \leq 10^2\varepsilon, \quad n > 0, \tag{4.1}
$$

where ε is the tolerance used for the matrix solver. Similar quantities are defined for the other variables. We note that these quantities are related to the time-derivative of the solution and therefore should become smaller as the solution does not change much in time and converges.

4.1. Numerical experiments

In this section we will present numerical simulations of the coupled system of BSRDEs on three different volumes: a sphere of

radius one, a cube of length one and a triaxial ellipsoid with semi-axis of lengths 1, 2 and 3. In all our simulations we fix $\gamma_\Omega = \gamma_\Gamma = 500$ and vary the diffusion coefficients as shown in Table 2. The numbers of degrees of freedom for the sphere were 59 042/3076 (bulk/surface), for the cube 71 874/12 292 and for the ellipsoid 59 042/3076. The timestep chosen in each case was $\tau = 10^{-3}$.

Remark 4.1. In [21] we exhibited a wide variety of patterns in the bulk and on the surface of the sphere of radius 1. We will omit some of these results and refer the interested reader to see [21].

Our numerical simulations reveal the following fundamental characteristics key to the theory of pattern formation:

1. By taking $d_\Omega = 1$ in the bulk and $d_\Gamma = 1$ on the surface, no patterns emerge (results not shown). This implies that the system fails to satisfy one of the necessary conditions for the formation of spatial structure which requires that one of the molecular species must diffuse much faster (typically the inhibitor) than the other (typically the activator), resulting in what is known as the *long-range inhibition short-range activation* [10,16]. This entails that both the bulk and surface dynamics are not able to generate patterns, instead the uniform steady state is the only stable solution.
2. Taking $d_\Omega = 1$ in the bulk and $d_\Gamma \gg 1$ on the surface, the bulk reaction–diffusion system is not able to generate patterns everywhere in the bulk. However, the surface reaction–diffusion system is able to form patterns on the surface as well as inducing patterning in a small band (which we can be considered as an epidermis) inside the bulk, close to the surface (see Figs. 3 and 5).
3. On the other hand, taking $d_\Omega \gg 1$ in the bulk and $d_\Gamma = 1$ on the surface, the bulk reaction–diffusion system is now able to generate patterns everywhere in the bulk including on the surface. The surface reaction–diffusion system generates patterns with small amplitudes (which seem to appear uniformly) compared to those in the bulk with large amplitudes (see Fig. 6).
4. If we take $d_\Omega \gg 1$ in the bulk and $d_\Gamma \gg 1$ on the surface, then the coupled bulk-surface reaction–diffusion system generates patterns in the interior as well as on the surface (see Figs. 7–9).
5. The evolution of the patterning forming process is characterised by three fundamental stages as shown in Figs. 2 and 4 where we

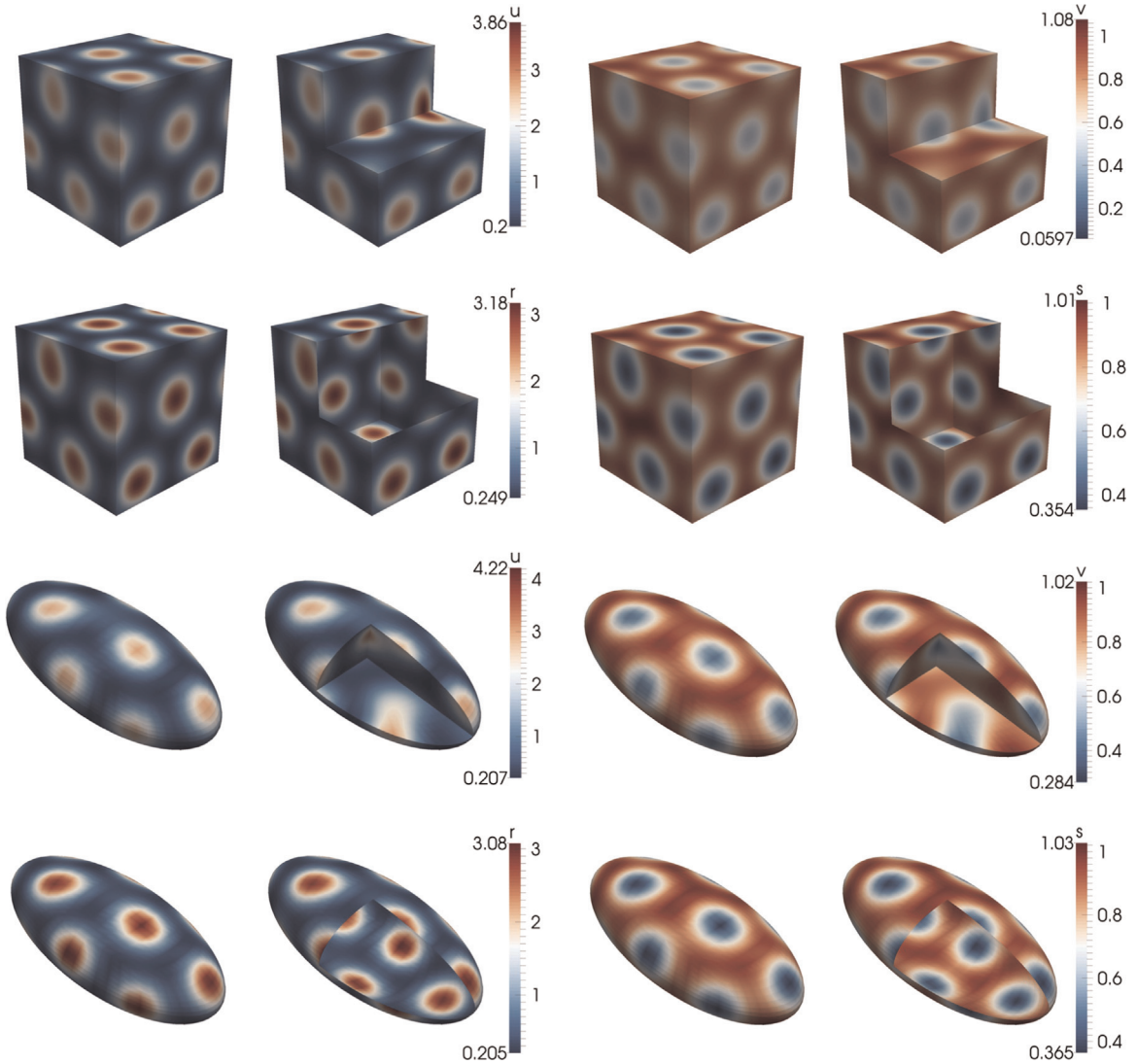

Fig. 9. Numerical solutions corresponding to the coupled system of BSRDEs (2.1)–(2.6) with $d_\Omega = 20$ in the bulk, $d_\Gamma = 20$ on the surface and $\gamma_\Omega = \gamma_\Gamma = 500$. Patterning behaviour is more complex for large values of the diffusion coefficients. Rows 2 and 4: solutions on the surface representing r and s . Second and fourth columns represent cross sections of the bulk and the surface respectively.

plot the L_2-norms of the errors of the numerical solutions. First, an initial stage that is characterised by a rapid decay due to the smoothing effects of diffusion. If no wavenumbers are excited, the decaying convergence process persists until a uniform steady state is converged to (see Fig. 2). On the other hand, if there are some excitable wavenumbers, then a second intermediate stage emerges which is characterised by an exponential growth of the positive excitable wavenumbers to induce the formation of spatial structure. It is during this phase that the uniform steady state is driven unstable. A third and final stage is when the nonlinear terms kick-in and become dominant to act as bounds for the exponentially growing modes resulting in the formation of a spatially stable inhomogeneous state corresponding to the coupled system of BSRDEs (2.1)–(2.6) (see Fig. 4). This evolution process is valid for all parameter values capable of inducing the formation of spatial structure for reaction–diffusion type models [16].

The results obtained are independent of the geometry; the sphere, cube and ellipsoid volumes all exhibit similar results. Furthermore, our results hold true for different values of the diffusion coefficients d_Ω in the bulk and d_Γ on the surface (further results not shown), and the scaling parameters γ_Ω and γ_Γ (further results not shown). Taking large values of γ_Ω and γ_Γ results in more complex patterns forming while for the same values of the diffusion coefficients as detailed above, similar patterning behaviour is observed.

5. Conclusion, discussion and future research challenges

In this study we have presented the bulk-surface finite element method for solving reaction–diffusion systems posed in the interior (bulk) of three-dimensional volumes as well as on the surface enclosing the volume. In doing so, we have set up a theoretical and computational framework that allows us to model more complex and experimentally driven models coupling interior and surface dynamics. In particular, new models can be derived in developmental biology and cell motility where such processes are experimentally supported.

In an earlier study [21], stability analytical theory was carried out to establish the conditions that give rise to the formation of spatial structure for such models (known as Turing diffusion-driven instability [29]) and this work supports the theoretical observations published. Our most revealing results are:

- In the absence of diffusion-driven instability in the interior, the surface reaction–diffusion system is able to generate patterns on the surface as well as in a small region inside the volume. This is biologically plausible, since patterns form on the skin as well as within the epidermis region adjacent to the skin surface.
- In the absence of diffusion-driven instability on the surface, the bulk reaction–diffusion system has the capability to induce patterns in the interior as well as on the surface.

The bulk-surface finite element method is inspired by the work of Elliott and Ranner [9] who were the first to introduce the method to study elliptic parabolic systems. For the first time, we have applied the bulk-surface finite element method to study time-dependent semi-linear parabolic partial differential equations in the form of reaction–diffusion. Within this framework, we have defined the surface triangulation as the trace of the bulk triangulation [17].

A natural extension of this study involves the introduction of surface evolution to study bulk-surface reaction–diffusion systems on three-dimensional evolving volumes. There are several ways to deal with mesh movement under this framework. For example, a spring type analogy could be used to deform the bulk mesh once the surface mesh has been evolved under some mechanism. In this case, the degrees of freedom for the mesh connectivity will remain unchanged. An alternative method is to introduce mesh adaptivity. This form is harder to implement since one must introduce mesh adaptivity strategies based on a priori as well as a posteriori error estimates. These extensions form part of our current studies.

Acknowledgements

This work (A.M.) is supported by the following grants: the Engineering and Physical Sciences Research Council (EP/J016780/1) on *Modelling, analysis and simulation of spatial patterning on evolving biological surfaces* and the Leverhulme Trust research project grant (RPG-2014-149) on *Unravelling new mathematics for 3D cell migration*. This project (A.M.) has received funding from the European Union's Horizon 2020 research and innovation programme under the Marie Sklodowska-Curie grant agreement no. 642866. The final writing up of this article was undertaken when A.M. was programme organiser of the Isaac Newton Institute for Mathematical Sciences 6-months programme on *Coupling geometric PDEs with physics for cell morphology, motility and pattern formation* (13 July–18 December 2015). This work (A.M.) was partially supported by a grant from the Simons Foundation. A.H.C.'s studies are supported partly by the University of Sussex and partly by the Medical Research Council. The authors thank the University of Sussex ITS and the School of Mathematics and Physical Sciences for providing computing clusters on which computations were carried out.

References

[1] W. Bangerth, T. Heister, L. Heltai, G. Kanschat, M. Kronbichler, M. Maier, B. Turcksin, T.D. Young, The `deal.ii` library, version 8.1. arXiv preprint arXiv:1312.2266, 2013.
[2] E. Bänsch, A. Schmidt, Simulation of dendritic crystal growth with thermal convection, Interfaces Free Bound 2 (1) (2000) 95–115.
[3] M. Booty, M. Siegel, A hybrid numerical method for interfacial fluid flow with soluble surfactant, J. Comput. Phys. 229 (10) (2010) 3864–3883.
[4] E. Burman, P. Hansbo, M. Larson, S. Zahedi, Cut finite element methods for coupled bulk-surface problems, Numer. Math. (2014) http://dx.doi.org/10.1007/s00211-015-0744-3.
[5] D.A. Calhoun, C. Helzel, A finite volume method for solving parabolic equations on logically cartesian curved surface meshes, SIAM J. Sci. Comput. 31 (6) (2009) 4066–4099.
[6] A.V. Chechkin, I.M. Zaid, M.A. Lomholt, I.M. Sokolov, R. Metzler, Bulk-mediated diffusion on a planar surface: full solution, Phys. Rev. E 86 (4) (2012) 041101.
[7] G. Dziuk, C.M. Elliott, Surface finite elements for parabolic equations, J. Comput. Math. 25 (4) (2007) 385.
[8] C. Elliott, T. Ranner, Finite element analysis for a coupled bulk-surface partial differential equation, IMA J. Numer. Anal. 33 (2013) 377–402.
[9] C.M. Elliott, T. Ranner, Finite element analysis for a coupled bulk–surface partial differential equation, IMA J. Numer. Anal. (2012) 1–26, http://dx.doi.org/10.1093/imanum/drs022.
[10] A. Gierer, H. Meinhardt, A theory of biological pattern formation, Kybernetik 12 (1) (1972) 30–39.
[11] J.B. Greer, A.L. Bertozzi, G. Sapiro, Fourth order partial differential equations on general geometries, J. Comput. Phys. 216 (1) (2006) 216–246.
[12] S. Gross, M.A. Olshanskii, A. Reusken, A trace finite element method for a class of coupled bulk-interface transport problems, ESAIM: Math. Modell. Numer. Anal. 9 (5) (2015) 1303–1330.
[13] J.J. Heys, T.A. Manteuffel, S.F. McCormick, J. Ruge, First-order system least squares (fosls) for coupled fluid-elastic problems, J. Comput. Phys. 195 (2) (2004) 560–575.
[14] S.E. Hieber, P. Koumoutsakos, A Lagrangian particle level set method, J. Comput. Phys. 210 (1) (2005) 342–367.
[15] A.B. Jaffe, A. Hall, Rho gtpases: biochemistry and biology, Annu. Rev. Cell Dev. Biol. 21 (2005) 247–269.
[16] J.D. Murray, Mathematical Biology II: Spatial Models and Biomedical Applications, third edition, Springer-Verlag, New York, 2003.
[17] D. Köster, O. Kriessl, K.G. Siebert, Design of Finite Element Tools for Coupled Surface and Volume Meshes, Technical Report 2008-01, Mathematik, 2008.

[18] C.B. Macdonald, B. Merriman, S.J. Ruuth, Simple computation of reaction–diffusion processes on point clouds, Proc. Natl. Acad. Sci. 110 (23) (2013) 9209–9214.
[19] C.B. Macdonald, S.J. Ruuth, The implicit closest point method for the numerical solution of partial differential equations on surfaces, SIAM J. Sci. Comput. 31 (6) (2009) 4330–4350.
[20] A. Madzvamuse, A.H. Chung, Fully implicit time-stepping schemes and non-linear solvers for systems of reaction–diffusion equations, Appl. Math. Comput. 244 (2014) 361–374.
[21] A. Madzvamuse, A.H. Chung, C. Venkataraman, Stability analysis and simulations of coupled bulk-surface reaction–diffusion systems, Proc. R. Soc. A 471 (20140546) (2015).
[22] E.S. Medvedev, A.A. Stuchebrukhov, Mechanism of long-range proton translocation along biological membranes, FEBS Lett. 587 (4) (2013) 345–349.
[23] D.R. Nisbet, A.E. Rodda, D.I. Finkelstein, M.K. Horne, J.S. Forsythe, W. Shen, Surface and bulk characterisation of electrospun membranes: problems and improvements, Colloids Surf. B 71 (1) (2009) 1–12.
[24] I.L. Novak, F. Gao, Y.-S. Choi, D. Resasco, J.C. Schaff, B.M. Slepchenko, Diffusion on a curved surface coupled to diffusion in the volume: application to cell biology, J. Comput. Phys. 226 (2) (2007) 1271–1290.
[25] I. Prigogine, R. Lefever, Symmetry breaking instabilities in dissipative systems. ii, J. Chem. Phys. 48 (4) (1968) 1695–1700.
[26] A. Rätz, M. Röger, Turing instabilities in a mathematical model for signaling networks, J. Math. Biol. 65 (6–7) (2012) 1215–1244.
[27] A. Rätz, M. Röger, Symmetry breaking in a bulk-surface reaction–diffusion model for signaling networks, Nonlinearity 27 (8) (2014) 1805, http://dx.doi.org/10.1088/0951–7715/27/8/1805.
[28] J. Schnakenberg, Simple chemical reaction systems with limit cycle behaviour, J. Theor. Biol. 81 (3) (1979) 389–400.
[29] A.M. Turing, The chemical basis of morphogenesis, Philos. Trans. R. Soc. B 237 (641) (1952) 37–72.